Modelling of cable-driven continuum robots with multiple generally routed cables

Soumya Kanti Mahapatra[1] and Ashitava Ghosal[1*]

[1]Department of Mechanical Engineering, Indian Institute of Science, Bangalore 560012, Karnataka, India.

*Corresponding author(s). E-mail(s): asitava@iisc.ac.in;
Contributing authors: soumyam@iisc.ac.in;

Abstract

Cable-driven continuum robots (CCR) are increasingly gaining traction in a wide array of practical applications when compared to their rigid-link counterparts. This paper presents a geometry-based optimization method to model a CCR with multiple generally routed cables. The method discretizes the CCR into equal sections and then assumes imaginary four bars in each section. The optimization is stated as the minimization of the coupler angles of these four bars as well as the angles made by tangents. Simulation results are shown for three different cases, which were compared with results obtained from a Cosserat rod model simulation. The maximum RMS error between the two methods is seen to be 1.57 mm (less than 0.88 % of the total length of the CCR), which verifies the accuracy of the proposed method. The average simulation time is also significantly faster in the case of the optimization-based method. This method can be used as a quick tool to study CCR's with diverse cable routings and arrangements.

Keywords: Cable-driven Continuum Robots, Flexible robot, General cable routing, Multiple cables

1 Introduction

Continuum robots have gained increasing prominence in real-world applications owing to their advantageous characteristics, including inherent compliance, lightweight design, and enhanced maneuverability. The fundamental structure of these robots primarily comprises a flexible backbone that can be actuated by various means, such as pneumatics, shape memory alloys, pre-curved beams, and cables [1]. Of all the types,

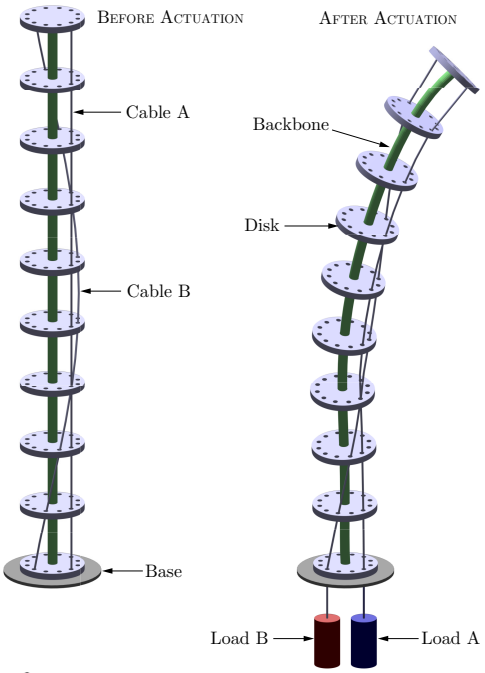

Fig. 1: Schematics of a CCR with two cables before and after actuation.

continuum robots actuated by cable are much preferred for their simple construction and ease of operation. Due to this, CCR finds usage in various fields, such as medical devices, space operations, biomimetics, and search and rescue, to name a few.

These Cable-driven Continuum Robots (CCR) consist of a rod-like structure called the *backbone* to which circular disks are attached at equal intervals (see Fig. 1 for reference). These disks have perforations in them through which one or more cables can be passed from the base to the tip. When the cables are actuated from the base, the CCR backbone deforms and attains a shape in three dimensions. The final shape is dictated by the routing of the cables.

Various models are available in literature whose detailed review can be found in [1–4]. These models range from simple constant curvature modelling for single section [5] and multiple sections [6] to more detailed material-based modelling. Cosserat rod models [7–9] have shown to model CCR with multiple generally routed cables with good accuracy, even with external loading. More recently, a finite element method (FEM) based model [10] is proposed for CCR mimicking skeletal spine with variable curvature. A statics-based model based on Euler-Bernoulli beam theory [11, 12] is shown to model CCR with multiple sections, taking into account gravity and cable friction along with external loading. Energy-based methods such as Euler-Lagrange formulation [5, 13], virtual-work [14] and virtual-power [15] has also been proposed. More recently, an optimization-based model is presented [16, 17], which has shown to model CCR with general cable routing and also work with obstacles in the workspace.

Although more such models are available, very few address the modelling of CCR with multiple generally routed cables. In this paper, we present a novel optimization-based model that can simulate the shape and pose of a CCR with multiple generally routed cables. This method is purely geometry-based, making it easier to use. The simulated results are compared with the well-known Cosserat rod model to check for accuracy. The rest of the paper is organized as follows – in section 2, the mathematical details of the method are presented, which is simulated in section 3, along with a comparison to the Cosserat rod model. Finally, in section 4, concluding remarks and scopes of future work is presented.

2 Methodology

This section presents details of the optimization-based method, which is based on the previous work in [16]. For nomenclature used[1,2], refer to Table 1.

Table 1: Nomenclature used in the formulation.

Symbol	Description
n	Number of backbone segments (= number of disks -1).
r	Radial distance from the center of the disk to the cable.
l_0	Length of a backbone segment.
l_a^i	Length of cable A after actuation in section i.
l_b^i	Length of cable B after actuation in section i.
Δ_{lA}	Percentage change in length of cable A after actuation.
Δ_{lB}	Percentage change in length of cable A after actuation.
$\mathbf{X}_0^i$	Position of backbone at the i^{th} disk in undeformed state (or previous iteration).
$\mathbf{X}_a^i$	Position of cable A at the i^{th} disk in unactuated state (or previous iteration).
$\mathbf{X}_b^i$	Position of cable B at the i^{th} disk in unactuated state (or previous iteration).
$\mathbf{x}_0^i$	Position of the deformed backbone at the i^{th} disk.
$\mathbf{x}_a^i$	Position of the actuated cable A at the i^{th} disk.
$\mathbf{x}_a^i$	Position of the actuated cable B at the i^{th} disk.
θ^i	Angle between cable B and cable A with respect to disk center at the i^{th} disk.
ϕ_a^i	Angular change of position of cable A with respective to the previous disk.
ϕ_b^i	Angular change of position of cable B with respective to the previous disk.
F_a	Force on cable A (for Cosserat rod model.)
F_b	Force on cable B (for Cosserat rod model.)

The CCR is discretized into n sections spanning between two disks (numbered 0 to n). The optimization problem is solved one section at a time iteratively. Starting for the first section ($i = 1$), one can assume two four bars which consist of vertices $\mathbf{X}_0^{i-1}\,\mathbf{X}_a^{i-1}\,\mathbf{X}_a^i\,\mathbf{X}_0^i$, and $\mathbf{X}_0^{i-1}\,\mathbf{X}_b^{i-1}\,\mathbf{X}_b^i\,\mathbf{X}_0^i$ (see Fig. 2a). In these two four-bars, $\mathbf{X}_0^{i-1}\,\mathbf{X}_a^{i-1}$, and $\mathbf{X}_0^{i-1}\,\mathbf{X}_b^{i-1}$ are the bases, $\mathbf{X}_0^{i-1}\,\mathbf{X}_0^i$ is the first crank for both, and $\mathbf{X}_0^i\,\mathbf{X}_a^i$, and $\mathbf{X}_0^i\,\mathbf{X}_b^i$ are the couplers. The vertices $\mathbf{X}_0^i$, $\mathbf{X}_a^i$, and $\mathbf{X}_b^i$ changes to $\mathbf{x}_0^i$, $\mathbf{x}_a^i$ and $\mathbf{x}_b^i$ respectively after actuation (See Fig. 2b). These new variables now become the base for the four bars for the next section.

It was shown that the pose of the CCR can be determined by minimizing the coupler angles [16]. The same idea is applied here, but the second four-bar is not

[1]The superscript denotes disk number, not an exponent.
[2]All the position vectors are defined from the center of the base disk (Global reference frame).

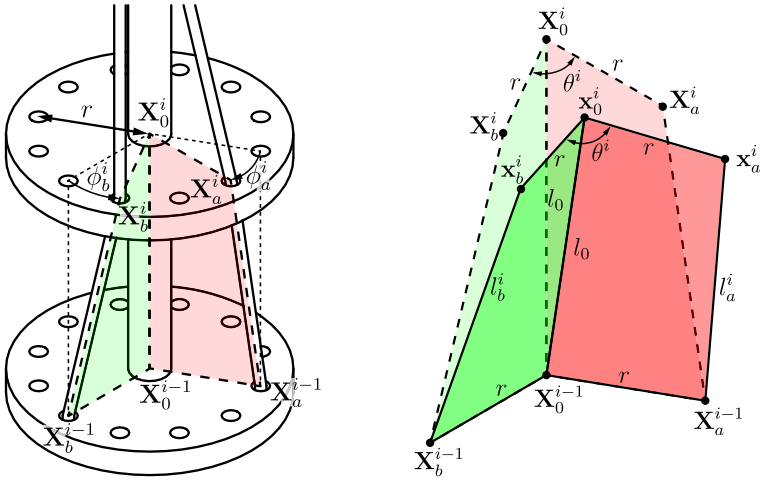

(a) (b)

Fig. 2: Nomenclature used for (a) i^{th} undeformed section (b) two four-bars before (lightly shaded) and after actuation (shaded dark). (All angles are measured counter-clockwise positive)

imaginary here. These two terms can be thought of as the minimization of the angle made by the normal vectors to the curve. The term related to the tangent vector [17] is also added to the final optimization problem, which can be stated as –

$$\begin{aligned}\underset{\mathbf{x}_0^i,\mathbf{x}_a^i,\mathbf{x}_b^i}{\arg\min} \quad & \left[\arccos\left(\frac{\mathbf{X}_a^i-\mathbf{X}_0^i}{\|\mathbf{X}_a^i-\mathbf{X}_0^i\|}\cdot\frac{\mathbf{x}_a^i-\mathbf{x}_0^i}{\|\mathbf{x}_a^i-\mathbf{x}_0^i\|}\right)+\right.\\ \left.\arccos\left(\frac{\mathbf{X}_b^i-\mathbf{X}_0^i}{\|\mathbf{X}_b^i-\mathbf{X}_0^i\|}\cdot\frac{\mathbf{x}_b^i-\mathbf{x}_0^i}{\|\mathbf{x}_b^i-\mathbf{x}_0^i\|}\right)+\arccos\left(\frac{\mathbf{X}_0^i-\mathbf{X}_0^{i-1}}{\|\mathbf{X}_0^i-\mathbf{X}_0^{i-1}\|}\cdot\frac{\mathbf{x}_0^i-\mathbf{X}_0^{i-1}}{\|\mathbf{x}_0^i-\mathbf{X}_0^{i-1}\|}\right)\right]\end{aligned} \tag{1}$$

Subject to:

$$\begin{aligned}&\|\mathbf{x}_0^i-\mathbf{X}_0^{i-1}\|=l_0,\quad \|\mathbf{x}_a^i-\mathbf{X}_a^{i-1}\|=l_a^i,\quad \|\mathbf{x}_b^i-\mathbf{X}_b^{i-1}\|=l_b^i,\quad \|\mathbf{x}_a^i-\mathbf{x}_0^i\|=r,\\ &\|\mathbf{x}_b^i-\mathbf{x}_0^i\|=r,\quad \text{and}\quad \arccos\left(\frac{\mathbf{x}_a^i-\mathbf{x}_0^i}{\|\mathbf{x}_a^i-\mathbf{x}_0^i\|}\cdot\frac{\mathbf{x}_b^i-\mathbf{x}_0^i}{\|\mathbf{x}_b^i-\mathbf{x}_0^i\|}\right)=\theta^i\end{aligned} \tag{2}$$

Given data: $\mathbf{X}_0^{i-1}$, $\mathbf{X}_0^i$, $\mathbf{X}_a^i$, $\mathbf{X}_b^i$, l_0, l_a^i, l_b^i, r and, θ_i.

To find out $\mathbf{X}_0^i$, $\mathbf{X}_a^i$, $\mathbf{X}_b^i$ we employ the following steps –

1. Assume $\hat{\boldsymbol{i}}$ along $\rightarrow \left(\mathbf{X}_a^{i-1}-\mathbf{X}_0^{i-1}\right)$.
2. Assume $\hat{\boldsymbol{j}}'$ along $\rightarrow \text{sign}(\theta^i)\left(\mathbf{X}_b^{i-1}-\mathbf{X}_0^{i-1}\right)$.
3. $\hat{\boldsymbol{k}}=\hat{\boldsymbol{i}}\times\hat{\boldsymbol{j}}'$, $\hat{\boldsymbol{j}}=\hat{\boldsymbol{k}}\times\hat{\boldsymbol{i}}$, and $\mathbf{T}=\begin{bmatrix}\hat{\boldsymbol{i}} & \hat{\boldsymbol{j}} & \hat{\boldsymbol{k}} & \mathbf{X}_0^{i-1}\\ 0 & 0 & 0 & 1\end{bmatrix}$

4. $\left[\mathbf{X}_0^i, 1\right] = \mathbf{T}\begin{bmatrix}\mathbf{d}\\1\end{bmatrix}$, $\left[\mathbf{X}_a^i, 1\right] = \mathbf{T}\begin{bmatrix}R_z(\phi_a^i) & \mathbf{d}\\0\ 0\ 0 & 1\end{bmatrix}\begin{bmatrix}\mathbf{X}_a^0\\1\end{bmatrix}$, and $\left[\mathbf{X}_b^i, 1\right] = \mathbf{T}\begin{bmatrix}R_z(\phi_a^i+\theta^i) & \mathbf{d}\\0\ 0\ 0 & 1\end{bmatrix}\begin{bmatrix}\mathbf{X}_a^0\\1\end{bmatrix}$, with $\mathbf{d} = \begin{bmatrix}0\\0\\l_0\end{bmatrix}$ – assuming $\widehat{\mathbf{X}_a^0} = \begin{bmatrix}1\\0\\0\end{bmatrix}$.

The equations in 2 preserve the geometric shape and limitations of the CCR. It is to be noted that all the angles are taken counter-clockwise positive, so the last equation in 2 should be carefully computed – the sign of $\theta^i \left(= \phi_b^i - \phi_a^i\right)$ will change when the cables cross over. The optimization-based method is solved one section at a time, starting from the base till the tip, where the outputs of the optimization problem form the base of the four bars for the next section.

3 Simulation

This section presents numerical simulations for the optimization-based method. These results are compared to the Cosserat rod model [8] simulations. For the simulations, the chosen dimensions and properties of the CCR (taken from [18]) were – $l_0 = 20\,\text{mm}$, $r = 8\,\text{mm}$ and, $n = 9$ (10 disks), $E = 1.1\,\text{GPa}$, $\nu = 0.3$, and $d = 3\,\text{mm}$. The geometry-based optimization method in equation 1 is solved using `fmincon` function with the in-built *interior-point algorithm* in MATLAB®. At each step, three coordinates are solved for a total of 27 coordinates.

The boundary value problem of the Cosserat rod model is solved using the *shooting method* for a total of 18 state variables. The cable positions $\boldsymbol{r}_i(s)$ are provided as an 8^{th} order Fourier approximations to make sure it is $\mathcal{C}^2$ continuous over the whole length.

The initial guesses were provided for both models, assuming the CCR is initially straight with no actuation. Out of multiple trials, three representative cases are presented here –

1. Case I - Both cables going straight up
   - $\mathbf{X}_a^i = [r,\, 0,\, il_0]^T, \quad \Delta_{la} = 4\%, \quad F_a = 425\,\text{g}$
   - $\mathbf{X}_b^i = \left[r\cos\frac{2\pi}{3},\, r\sin\frac{2\pi}{3},\, il_0\right]^T, \quad \Delta_{lb} = 3\%, \quad F_b = 390\,\text{g}$
2. Case II - One cable straight and one non-straight
   - $\mathbf{X}_a^i = \left[r\cos\frac{i\pi}{6},\, r\sin\frac{i\pi}{6},\, il_0\right]^T, \quad \Delta_{la} = 2.5\%, \quad F_a = 80\,\text{g}$
   - $\mathbf{X}_b^i = \left[r\cos\frac{7\pi}{12},\, r\sin\frac{7\pi}{12},\, il_0\right]^T, \quad \Delta_{lb} = 3\%, \quad F_b = 135\,\text{g}$
3. Case III - Both cables are non-straight
   - $\mathbf{X}_a^i = \left[r\cos\frac{i\pi}{6},\, r\sin\frac{i\pi}{6},\, il_0\right]^T, \quad \Delta_{la} = 3\%, \quad F_a = 105\,\text{g}$
   - $\mathbf{X}_b^i = \left[r\cos\left(\frac{\pi}{2}+\phi(i)\right),\, r\sin\left(\frac{\pi}{2}+\phi(i)\right),\, il_0\right]^T, \quad \Delta_{lb} = 2\%, \quad F_b = 190\,\text{g}$

$$\text{where, } \phi(i) = \frac{i\pi}{6}, \qquad i \leq 3$$
$$= \frac{i\pi}{2}, \qquad 3 < i \leq 6$$
$$= \frac{(i-3)\pi}{6}, \qquad i > 6$$

The simulations were performed in a PC with an Intel processor (2.60 GHz) and 24 GB RAM, taking on an average of 2.08 seconds for the optimization-based method and 7.13 seconds for the Cosserat rod model. The average simulation times are faster as compared to the Cosserat rod model, which is consistent with [18]. The simulation results are presented in Fig. 3. It can be seen from the figures that both the results match very closely with their RMS errors as 1.57 mm, 1.52 mm, and 1.19 mm for the Cases I, II, and III respectively.

4 Conclusion

In this paper, a geometry-based optimization is used to model CCR with multiple generally routed cables. The method is purely geometry-based, eliminating the usage of material properties. This makes the usage of the method more simpler. The formulation uses displacement as the actuation method, which is much easier to measure rather than force, which is usually used in other formulations. The simulated results were compared to the well-known Cosserat rod model, which showed a maximum RMS error of 1.57 mm, which is less than 0.88 % of the total length of the CCR. The average simulation times for the optimization-based method are also significantly faster than the Cosserat rod model.

Experimental validations of the results, as well as kinematics in the presence of obstacles, are a work in progress.

References

[1] Webster, R.J., Jones, B.A.: Design and kinematic modeling of constant curvature continuum robots: A review. The International Journal of Robotics Research **29**(13), 1661–1683 (2010)

[2] Chirikjian, G.S.: Conformational modeling of continuum structures in robotics and structural biology: A review. Advanced Robotics **29**(13), 817–829 (2015)

[3] Rao, P., Peyron, Q., Lilge, S., Burgner-Kahrs, J.: How to model tendon-driven continuum robots and benchmark modelling performance. Frontiers in Robotics and AI **7** (2021)

[4] Armanini, C., Boyer, F., Mathew, A.T., Duriez, C., Renda, F.: Soft robots modeling: A structured overview. IEEE Transactions on Robotics **39**(3), 1728–1748 (2023)

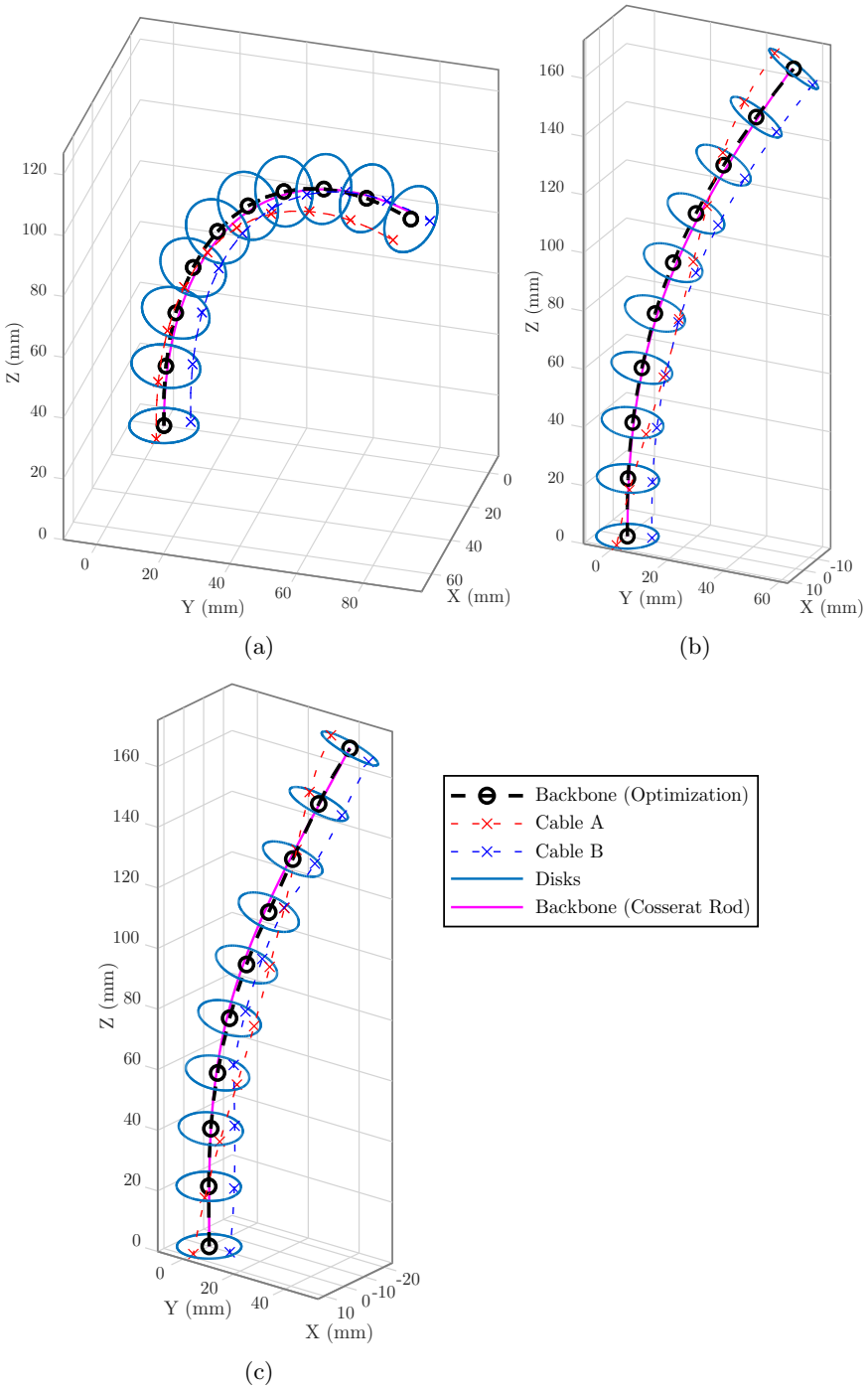

Fig. 3: Simulation results for (a) Case I, (b) Case II, and (c) Case III.

[5] Gravagne, I.A., Walker, I.D.: On the kinematics of remotely-actuated continuum robots. In: Proceedings 2000 ICRA. Millennium Conference. IEEE International Conference on Robotics and Automation. Symposia Proceedings (Cat. No.00CH37065), vol. 3, pp. 2544–2550. IEEE, New Jersey (2000)

[6] Cobos-Guzman, S., Palmer, D., Axinte, D.: Kinematic model to control the end-effector of a continuum robot for multi-axis processing. Robotica **35**(1), 224–240 (2017)

[7] Starke, J., Amanov, E., Chikhaoui, M.T., Burgner-Kahrs, J.: On the merits of helical tendon routing in continuum robots. In: 2017 IEEE/RSJ International Conference on Intelligent Robots and Systems (IROS), pp. 6470–6476. IEEE, New Jersey (2017)

[8] Rucker, D.C., Webster III, R.J.: Statics and dynamics of continuum robots with general tendon routing and external loading. IEEE Transactions on Robotics **27**(6), 1033–1044 (2011)

[9] Till, J., Aloi, V., Rucker, C.: Real-time dynamics of soft and continuum robots based on Cosserat rod models. The International Journal of Robotics Research **38**(6), 723–746 (2019)

[10] Morales Bieze, T., Kruszewski, A., Carrez, B., Duriez, C.: Design, implementation, and control of a deformable manipulator robot based on a compliant spine. The International Journal of Robotics Research **39**(14), 1604–1619 (2020)

[11] Yuan, H., Li, Z.: Workspace analysis of cable-driven continuum manipulators based on static model. Robotics and Computer-Integrated Manufacturing **49**, 240–252 (2018)

[12] Yuan, H., Zhou, L., Xu, W.: A comprehensive static model of cable-driven multi-section continuum robots considering friction effect. Mechanism and Machine Theory **135**, 130–149 (2019)

[13] Ehsani-Seresht, A., Hashemi-Pour Moosavi, S.: Dynamic modeling of the cable-driven continuum robots in hybrid position-force actuation mode. Journal of Mechanisms and Robotics **12**(5) (2020). : 051002

[14] Rone, W.S., Ben-Tzvi, P.: Continuum manipulator statics based on the principle of virtual work. In: Volume 4: Dynamics, Control and Uncertainty, Parts A and B. ASME International Mechanical Engineering Congress and Exposition, pp. 321–328 (2013)

[15] Liu, Z., Zhang, X., Cai, Z., Peng, H., Wu, Z.: Real-time dynamics of cable-driven continuum robots considering the cable constraint and friction effect. IEEE Robotics and Automation Letters **6**(4), 6235–6242 (2021)

[16] Ashwin, K.P., Ghosal, A.: Profile estimation of a cable-driven continuum robot with general cable routing. In: Mechanisms and Machine Science vol. 73, pp. 1879–1888. Springer, Cham (2019)

[17] Ashwin, K.P., Mahapatra, S.K., Ghosal, A.: Profile and contact force estimation of cable-driven continuum robots in presence of obstacles. Mechanism and Machine Theory **164**, 104404 (2021)

[18] Mahapatra, S.K., Ashwin, K.P., Ghosal, A.: Modelling of cable-driven continuum robots with general cable routing: A comparison. In: Advances in Asian Mechanism and Machine Science, pp. 345–353. Springer, Cham (2022)